Local isotropy of the velocity and vorticity fields in a boundary layer at high Reynolds numbers

James M. Wallace[1] and Lawrence Ong[2]
[1]*Department of Mechanical Engineering, Burgers Program for Fluid Dynamics, University of Maryland, College Park, Maryland 20742, USA*
[2]*Science Systems and Applications Inc., Code 614.4, National Aeronautics and Space Administration/ Goddard Space Flight Center, Greenbelt, Maryland 20771, USA*

(Received 14 December 2007; accepted 4 May 2008; published online 31 October 2008)

Measurements of the velocity and vorticity field with a 12-sensor hot-wire probe were carried out in the boundary layer of the test section ceiling of the NASA Ames 80×120 ft^2 wind tunnel at a turbulence Reynolds number of $R_\lambda\approx875$. Tests of local isotropy were applied to the data obtained at $y/\delta=0.1$. In the inertial subrange, which extended over a decade of wave numbers for this experiment, both the velocity and vorticity component one-dimensional k_x spectra agree well with the isotropic spectra of Kim and Antonia [J. Fluid Mech. **251**, 219 (1993)]. This agreement extends into the dissipation range up to wave numbers at which the accuracy of the measurements is limited because of spatial resolution and other sources of error. Additional tests of local isotropy, from the characteristics of the Reynolds shear stress correlation coefficient cospectrum and from the isotropic relationships between the k_x spectra of the streamwise velocity and vorticity components with the k_x spectra of the respective cross-stream components, also show evidence of local isotropy at these higher wave numbers. © *2008 American Institute of Physics*. [DOI: 10.1063/1.3005842]

I. INTRODUCTION

The hypothesis, first advanced by Kolmogorov,[1] that turbulence at large wave numbers is isotropic and has universal spectral characteristics which are independent of the flow geometry, at least for high Reynolds numbers, has been a cornerstone of closure theories as well as of the most promising development in the effort to predict turbulent flows, viz., large eddy simulations. Experimental measurements of the velocity field have frequently been made to verify this fundamental assumption. However, Van Atta[2] suggested that an examination of the scalar and velocity *gradient* fields is necessary to definitively verify this hypothesis and to determine its range of applicability.

Antonia *et al.*[3] showed that the one-dimensional k_x spectral densities of the velocity gradients that make up the vorticity components are related to the energy spectrum tensor by

$$E_{i,m}(k_x)=\int\int_{-\infty}^{\infty}k_m^2E_i(\mathbf{k})dk_ydk_z, \tag{1}$$

where $E_{i,m}$ is the spectral density of the respective velocity gradient components and E_i is the spectral density of the respective velocity components ($i=u$, v, or w and $m=x$, y, or z). Only for the special case where the flow is isotropic are relationships available that allow us to determine the cross-stream wave number integrals on the right-hand side of Eq. (1) in terms of the energy magnitude spectrum, $E(k)$, where $k=|\mathbf{k}|$. Thus, in general, the one-dimensional k_x spectra of the vorticity components are not derivable from the k_x spectra of the velocity components, and local isotropy of the vorticity field is therefore not implied by local isotropy of the velocity field.

Antonia and co-workers[3–5] used a hot-wire probe consisting of two X arrays separated in appropriate cross-stream directions to estimate velocity gradients and their spectra as well as spectra of vorticity components and dissipation rate determined from these gradients in a turbulent, self-preserving wake. They found spectral characteristics consistent with the idea of local isotropy at high wave numbers. Kim and Antonia[6] and Antonia and Kim[7] used the direct numerical simulation (DNS) of a channel flow with a Reynolds number of $R_\tau=395$ (based on the friction velocity u_τ and the channel half-width h) to examine the question of local isotropy. In spite of the low Reynolds number of the simulated flow, clear indications from several tests of local isotropy in both the velocity and vorticity fields were evident at high wave numbers. They[7] also examined databases from DNS of a homogeneous turbulent shear flow and a turbulent mixing layer and found local isotropy at high wave numbers when the mean strain rate was sufficiently small. Morris and Foss[8] compared the spanwise vorticity component spectra obtained from an experiment in the atmospheric surface layer at $y^+\approx2500$ and from a single stream mixing layer to a model isotropic spectrum. For wave numbers $k_x\eta<0.1$ the spectra exhibit a k_x^{-1} power law behavior which is not seen in the other experiments or DNS cited above.

Saddoughi and Veeravalli[9] performed experiments with single-sensor and small X-array hot-wire probes in the boundary layer of the upper wall of the NASA Ames 80 $\times120$ ft^2 wind tunnel at a streamwise station with a 50 m fetch for freestream speeds of 10 and 40 m/s. They examined the local isotropy of the velocity field by means of spectral relationships and structure function tests and found that it is attained for all the conditions they tested at $\epsilon^{1/2}S^{-3/2}k_x\approx10$,

FIG. 1. (Color online) Interior of the NASA Ames 80×120 ft^2 wind tunnel test section. Arrow indicates measurement station.

where ϵ is the dissipation rate and k_x is the streamwise wave number.

II. EXPERIMENTAL FACILITY AND INSTRUMENTATION

A. Wind tunnel

Our experiments were performed in parallel with the low-speed experiments of Saddoughi and Veeravalli[9] at the lower freestream speed of 10 m/s. This speed corresponds to a momentum thickness Reynolds number of $R_\theta \approx 74\,000$ and a turbulence Reynolds number of $R_\lambda \approx 875$ at $y/\delta \approx 0.1$, with the boundary layer thickness $\delta \approx 1.1$ m at our measurement station. Under these conditions the Kolmogorov length scale is estimated to be $\eta \approx 0.22$ mm from our direct measurements of the dissipation rate, $\epsilon \approx 1.39$ m^2 s^{-3}. The local mean velocity at this position in the boundary layer is $\bar{U}_{\text{local}} \approx 7.0$ m/s.

Our experiments were conducted at one of the side viewing ports on the ceiling of the wind tunnel, as indicated in Fig. 1, at approximately 50 m from the end of the contraction and about 6.6 m from the side wall. The airplane and people in the photograph of the interior of the tunnel test section indicate its size, but the tunnel was empty for these experiments. Any large scale anisotropies introduced by corner secondary flows and the rough wall of this wind tunnel only create a more stringent test for the local isotropy hypothesis. Measurements were made with the probe located at $y/\delta \approx 0.1$, 0.2, 0.3, 0.4, 0.5, 0.6, 0.7, and 1.6 from the ceiling of the wind tunnel. Only the data at the $y/\delta \approx 0.1$ location where the local mean shear rate is largest will be discussed here. The Reynolds shear stress profile given by Saddoughi and Veeravalli[9] shows that roughness effects are confined to the region below this location in this rough wall boundary layer.

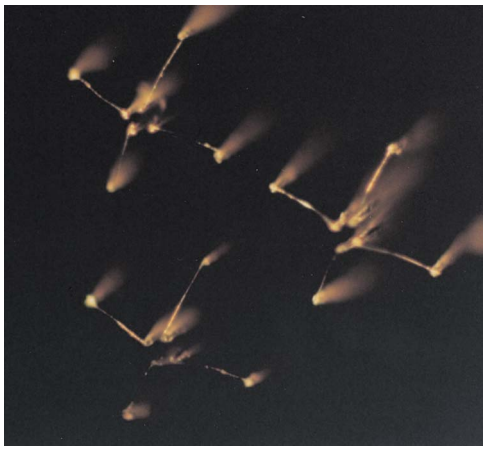

FIG. 2. (Color online) Photograph of the 12-sensor probe of Vukoslavčević and Wallace (Ref. 10). Each sensor is 0.5 mm long and is inclined at 45° to the flow.

B. Multisensor hot-wire probe

The 12-sensor probe used in this investigation and shown in the photograph of Fig. 2 was constructed and tested by Vukoslavčević and Wallace.[10] It consists of three arrays of four hot-wire sensors each. The sensors are contained within a small measuring region of about 2.5 mm diameter in the cross-stream plane.

1. Data acquisition

The hot-wire sensors were operated in the constant temperature mode at an overheat ratio of 1.2 with an A. A. Lab Systems 12-channel hot-wire anemometer system. The maximum sustainable throughput of our Optim Megadac 5017A data acquisition system was approximately 72 kHz, i.e., 6 kHz per channel when sampling 12 channels simultaneously. This relatively low sampling frequency could not sufficiently resolve the expected Kolmogorov frequency range, which was estimated to be approximately 4.5–5.5 kHz. In order to overcome this technical limitation, the outputs of the anemometer channels were initially analog recorded on FM tapes at 40 in./s providing a frequency response of approximately 20 kHz and later digitized individually. This method required a synchronization signal to be simultaneously recorded on the tape in order to uniquely identify a common trigger time for all the channels. A total of 13 channels (including the synchronization channel) was recorded at each measurement location for recording durations of 180 s.

2. Data reduction

The velocity vector $\mathbf{V}$ cooling each sensor can be written as

$$\mathbf{V} = U_n\mathbf{n} + U_b\mathbf{b} + U_t\mathbf{t}, \tag{2}$$

where $\mathbf{n}$, $\mathbf{b}$, and $\mathbf{t}$ are unit vectors in the normal, binormal, and tangential directions with respect to the sensor. Jorgensen's[11] law expresses the square of the "effective" velocity magnitude cooling the sensor as a weighted sum of the squares of these components,

$$U_e^2 = U_n^2 + h^2 U_b^2 + k^2 U_t^2, \tag{3}$$

where the respective weighting factors for the three components are unity, h^2, and k^2. The value of h depends on, among other influences, the aerodynamic blockage of the flow by the prongs and is usually close to unity. The value of k depends on the aspect ratio of the sensor, ℓ/d; for the $\ell/d \approx 200$ of the sensors used here, $k \approx 0.2$.

It is usually more convenient to decompose $\mathbf{V}$ into components in the laboratory coordinate system,

$$\mathbf{V} = U\mathbf{i} + V\mathbf{j} + W\mathbf{k}, \tag{4}$$

with unit vectors $\mathbf{i}$, $\mathbf{j}$, and $\mathbf{k}$ in the streamwise, wall normal, and spanwise (x, y, and z) directions, respectively. For an arbitrary orientation of $\mathbf{V}$, we can relate its two decompositions given in Eqs. (2) and (4) by

$$U_n = n_1 U + n_2 V + n_3 W, \tag{5}$$

$$U_b = b_1 U + b_2 V + b_3 W, \tag{6}$$

and

$$U_t = t_1 U + t_2 V + t_3 W, \tag{7}$$

where the coefficients n_i, b_i, and t_i ($i=1-3$) can be expressed in terms of sines and cosines of the angles of inclination of the sensors to the laboratory coordinate system axes. However, determining these angles is not necessary because these coefficients are incorporated into other coefficients that are determined by calibration, as shown below. If we now substitute for U_n, U_b, and U_t from Eqs. (5)–(7) into Eq. (3), we obtain for the jth sensor of a probe array a general expression for the effective velocity cooling the sensor in terms of the velocity components in the laboratory coordinate system,

$$U_{e_j}^2 = a_{1j} U_j^2 + a_{2j} V_j^2 + a_{3j} W_j^2 + a_{4j} U_j V_j + a_{5j} U_j W_j + a_{6j} V_j W_j, \tag{8}$$

where the coefficients a_{nj} ($n=1-6$) are products of the geometry coefficients, n_i, b_i, and t_i, in Eqs. (5)–(7) with the weighting factors, h and k, in Eq. (3).

Following Marasli *et al.*,[12] a polynomial in E_j, the voltage heating the jth sensor, given by

$$U_{e_j} = \sum_{m=1}^{q} A_{mj} E^{m-1}, \tag{9}$$

where A_{mj} are the qth-order polynomial coefficients of the jth sensor, is equated to $U_{e_j}^2$ in Eq. (8) to obtain

$$U_{e_j}^2 = P_j(E_j) = A_{1j} + A_{2j} E_j + A_{3j} E_j^2 + A_{4j} E_j^3 + A_{5j} E_j^4. \tag{10}$$

The coefficients a_{nj} in Eq. (8) and A_{mj} in Eq. (10) for each sensor are determined by calibration.

Because of the spatial variation in the velocity field, for any multisensor probe, the velocity components, U_j, V_j, and W_j, that cool each of the j sensors are different. Assuming that the gradients are constant within the probe measuring region at a given instant, the velocity components occurring at the midpoint of each sensor can be estimated from a Taylor series expansion to first order. This expansion about the geometric center of the probe in the cross-stream plane perpendicular to the probe axis and passing through the center of each sensor gives

$$U_j = U_o + C_j \frac{\partial U}{\partial y} + D_j \frac{\partial U}{\partial z}, \tag{11}$$

$$V_j = V_o + C_j \frac{\partial V}{\partial y} + D_j \frac{\partial V}{\partial z}, \tag{12}$$

and

$$W_j = W_o + C_j \frac{\partial W}{\partial y} + D_j \frac{\partial W}{\partial z}. \tag{13}$$

The coefficients C_j and D_j ($j=1-12$) represent the spanwise and vertical displacements, which must be accurately measured, of the centers of each of the sensors from the probe geometric center, and the velocity components, U_o, V_o, and W_o, are those at the probe geometric center. Substituting Eqs. (11) and (12) into Eq. (8) and neglecting gradient product terms, then replacing $U_{e_j}^2$ with this expression in Eq. (10) and rearranging yields 12 nonlinear algebraic equations with nine unknowns: the three velocity components, U_o, V_o, and W_o, and the six velocity gradients in the cross-stream plane, $\partial U/\partial y$, $\partial V/\partial y$, $\partial W/\partial y$, $\partial U/\partial z$, $\partial V/\partial z$, and $\partial W/\partial z$. These 12 equations ($j=1-12$) can be expressed as

$$\begin{aligned} f_j \equiv & -P_j + U_o^2 + 2C_j U_o \frac{\partial U}{\partial y} + 2D_j U_o \frac{\partial U}{\partial z} - k_{2j}\left[V_o^2 + 2C_j V_o \frac{\partial V}{\partial y} + 2D_j V_o \frac{\partial V}{\partial z}\right] - k_{3j}\left[W_o^2 + 2C_j W_o \frac{\partial W}{\partial y} + 2D_j W_o \frac{\partial W}{\partial z}\right] \\ & - k_{4j}\left[U_o V_o + C_j\left(U_o \frac{\partial V}{\partial y} + V_o \frac{\partial U}{\partial y}\right) + D_j\left(U_o \frac{\partial V}{\partial z} + V_o \frac{\partial U}{\partial z}\right)\right] - k_{5j}\left[U_o W_o + C_j\left(U_o \frac{\partial W}{\partial y} + W_o \frac{\partial U}{\partial y}\right) + D_j\left(U_o \frac{\partial W}{\partial z} + W_o \frac{\partial U}{\partial z}\right)\right] \\ & - k_{6j}\left[V_o W_o + C_j\left(V_o \frac{\partial W}{\partial y} + W_o \frac{\partial V}{\partial y}\right) + D_j\left(V_o \frac{\partial W}{\partial z} + W_o \frac{\partial V}{\partial z}\right)\right] = 0, \end{aligned} \tag{14}$$

where $k_{nj} = a_{nj}/a_{1j}$ ($n=2-6$).

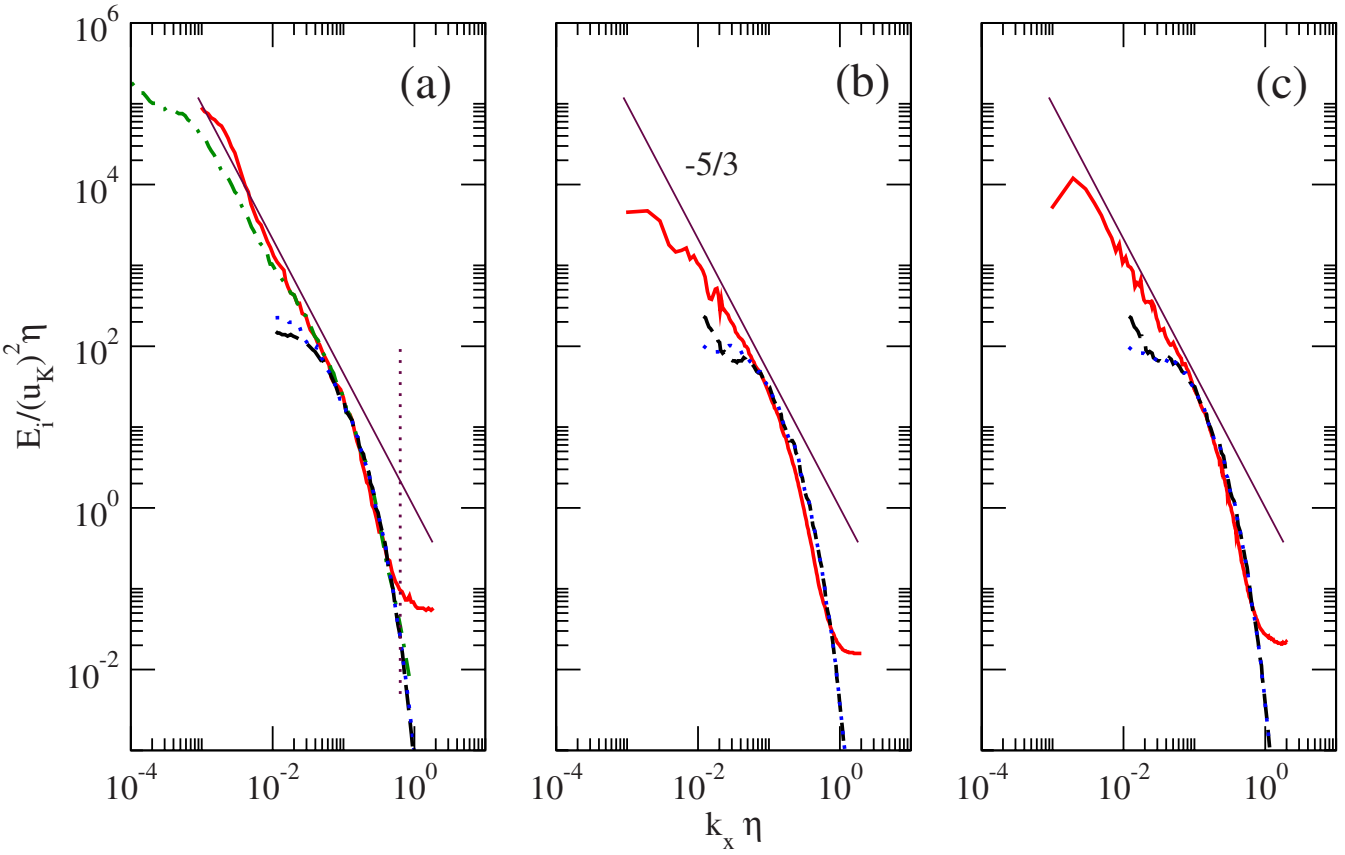

FIG. 3. (Color online) Velocity spectra: (a) streamwise component; (b) wall normal component; (c) spanwise component. (——) Present data; (—·—) Saddoughi and Veeravalli (Ref. 9); (···) channel flow DNS, Kim and Antonia (Ref. 6); (---) isotropic calculation from Eqs. (15) and (16), Kim and Antonia (Ref. 6). Vertical dotted line here and in other figures indicates the probe scale.

Equation (14) is solved at each time step by minimizing the error function given by Σf_j^2 $(j=1-12)$ using Newton's method. The streamwise gradients must be determined by transforming time derivatives into derivatives in the x direction using Taylor's[13] hypothesis. Its validity for bounded flows has been studied by Piomelli *et al.*,[14] who found that it provides good estimates of streamwise gradients this far from the bounding wall.

The underlying assumption of the first-order Taylor expansion about the probe geometric center is that the velocity gradient field is constant across the probe at any measurement instant. This is a reasonable assumption provided the smallest scales of the turbulent flow being measured are similar to or larger than the measuring volume of the 12-sensor probe. The spatial resolution of the 12-sensor probe was estimated to be about 10η, so some attenuation in the velocity gradient measurements occurs due to the breakdown of this assumption about the linear variation in the velocity field across the sensors.

III. RESULTS

A. Velocity and vorticity component spectra

The one-dimensional energy spectrum of the streamwise velocity component, $E_u(k_x\eta)$, calculated from this experiment and normalized with the Kolgomorov velocity and length scales, $u_k \equiv (\nu\epsilon)^{1/4}$ and $\eta \equiv (\nu^3/\epsilon)^{1/4}$, is shown in Fig. 3(a). Our E_u spectrum is compared to that of Saddoughi and Veeravalli[9] from measurements in the same wind tunnel under almost the same flow conditions. The experiments were carried out simultaneously but at different spanwise locations in the wind tunnel. For these experiments, over a decade of inertial subrange is evident. Our spectrum is also compared to that from the channel flow DNS of Kim and Antonia.[6] For this simulation, $R_\lambda = 53$ at the channel centerline where the spectrum shown was calculated. Compared as well is the one-dimensional isotropic spectrum calculated by Kim and Antonia[6] from the full three-dimensional spectrum as given by

$$E_u(k_x) = \frac{1}{2}\int_{k_x}^{\infty} \frac{E(k)}{k}\left(1 - \frac{k_x^2}{k^2}\right)dk. \tag{15}$$

As Kim and Antonia[6] found for their channel flow DNS $E_u(k_x)$ spectrum, our spectrum agrees with the calculated isotropic spectrum in the inertial subrange where there is overlap, as does that of Saddoughi and Veeravalli.[9] In the dissipation range the agreement continues to be good until the spectral density from our probe, which is considerably larger than that of the single-sensor probe of Saddoughi and Veeravalli,[9] begins to show a little attenuation for $k_x\eta > 0.2$. At $k_x\eta > 0.5$, aliasing and electronic noise cause our experimental spectrum to turn up.

The one-dimensional energy spectra from our experi-

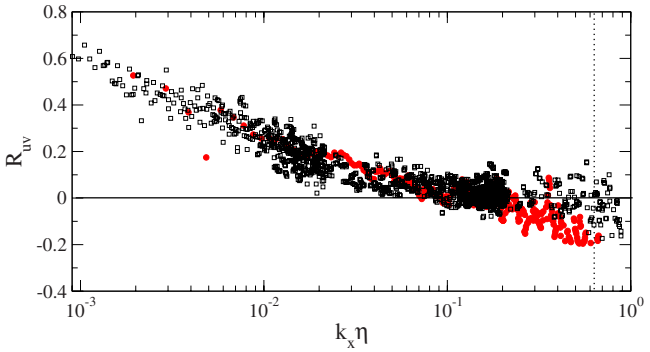

FIG. 4. (Color online) Reynolds shear stress cospectrum: (□) Saddoughi and Veeravalli (Ref. 9); (●, red online) present data.

ment and the DNS of Kim and Antonia[6] of the wall normal and spanwise velocity components $E_v(k_x\eta)$ and $E_w(k_x\eta)$, normalized with Kolmogorov scaling, are shown in Figs. 3(b) and 3(c). They are compared to the isotropic spectrum calculated by Kim and Antonia[6] using the DNS from the relationship

$$E_v(k_x) = E_w(k_x) = \frac{1}{2}\int_{k_x}^{\infty} \frac{E(k)}{k}\left(1 + \frac{k_x^2}{k^2}\right)dk. \tag{16}$$

As for the streamwise velocity component, our measured spectra of the wall normal and spanwise components agree well with the DNS channel flow spectra of Kim and Antonia[6] and their isotropic calculation in the inertial range where there is overlap, as well as in the dissipation range for $k_x\eta < 0.2$.

Similar to our streamwise velocity component spectrum, these cross-stream velocity component spectra display a little attenuation for $k_x\eta > 0.2$ in the dissipation range and turn upward at $k_x\eta \approx 0.5$. The wave number $k_x\eta \approx 0.63$, corresponding to the largest dimension over which gradients are estimated with the probe, i.e., 2.2 mm, is indicated in the figure as a vertical dotted line.

A sensitive test of local isotropy is the cospectrum of the Reynolds shear stress correlation coefficient,

$$R_{uv} = \frac{-E_{uv}(k_x)}{[E_u(k_x)E_v(k_x)]^{1/2}}, \tag{17}$$

where $\int_0^\infty E_{uv}(k_x)dk_x = -\overline{uv}$. In the wave number range where the flow is locally isotropic, R_{uv} must go to zero. Figure 4 shows the shear stress cospectrum measured with our 12-sensor probe compared to that of Saddoughi and Veeravalli.[9] The agreement is excellent. Both spectra go to zero at $k_x\eta \approx 0.1$, i.e., at the beginning of the dissipation range, which, for this location in the flow, is a nondimensional wave number based on the local mean shear rate of $\epsilon^{1/2}S^{-3/2}k_x \approx 5$, where $S = d\bar{U}/dy$. For $k_x\eta > 0.2$ our data drop below zero because of the measurement issues mentioned above.

With the data obtained in this experiment the one-dimensional spectra of the vorticity components could be obtained. These are shown in Figs. 5(a)–5(c). They are compared to the spectra obtained from the channel flow DNS of Kim and Antonia[6] and to their calculated isotropic spectra of the vorticity components using the relationships

$$E_{\omega_x}(k_x) = \frac{1}{2}\int_{k_x}^{\infty} \frac{E(k)}{k}(k^2 - k_x^2)dk \tag{18}$$

and

$$E_{\omega_y}(k_x) = E_{\omega_z}(k_x) = \frac{1}{2}k_x^2\int_{k_x}^{\infty} \frac{E(k)}{k}dk + \frac{1}{4}\int_{k_x}^{\infty} \frac{E(k)}{k}(k^2 - k_x^2)dk \tag{19}$$

or, equivalently,

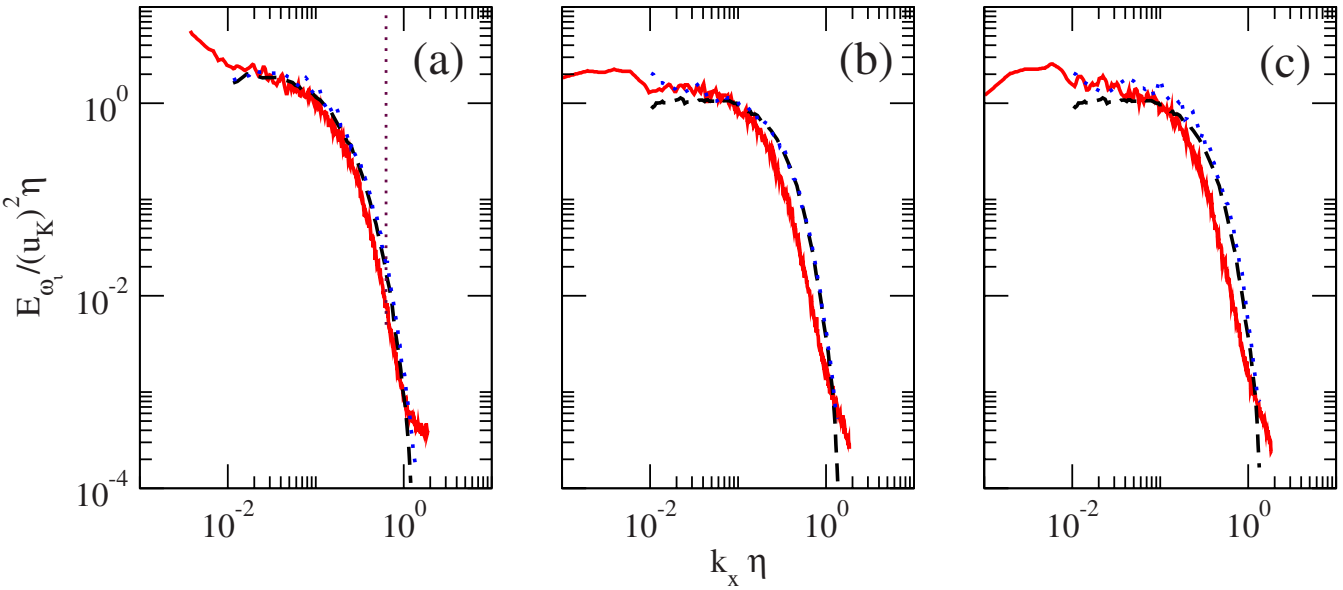

FIG. 5. (Color online) Vorticity spectra: (a) streamwise component; (b) wall normal component; (c) spanwise component. (——) Present data; (···) channel flow, Kim and Antonia (Ref. 6); (---) isotropic calculations from Eqs. (18) and (19), Kim and Antonia (Ref. 6).

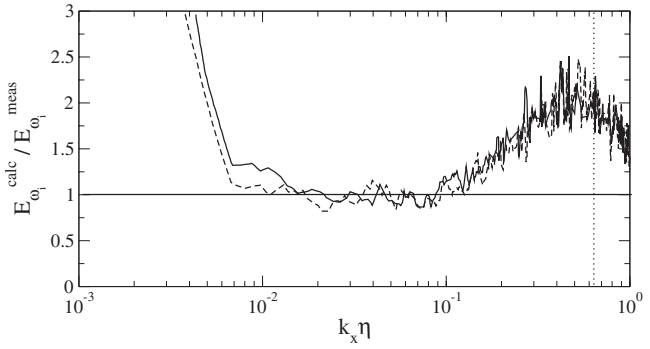

FIG. 6. Distributions of the ratios of wall normal and spanwise vorticity spectra calculated from Eq. (21) to their measured values: (——) $i=y$; (---) $i=z$.

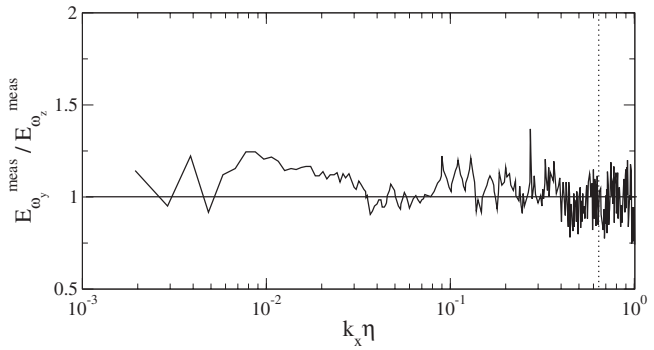

FIG. 7. Distribution of the ratio of measured wall normal to spanwise vorticity component spectra.

$$E_{\omega_y}(k_x) = E_{\omega_z}(k_x) = \frac{1}{4}\int_{k_x}^{\infty} \frac{E(k)}{k}(k^2 + k_x^2)dk, \tag{20}$$

as given by Antonia *et al.*[4] Our measured vorticity component spectra, those from the DNS of Kim and Antonia,[6] and their calculated isotropic spectra all agree quite well within the inertial subrange where there is overlap, the high wave number end of which is at $k_x\eta \approx 0.1$ [see Fig. 3(a)]. In the dissipation range for $k_x\eta > 0.2$ the energy in our spectra falls off more rapidly than in both the DNS and calculated isotropic spectra. This is due to probe spatial resolution effects and the fact that our velocity gradient approximation is a first-order finite difference, whereas the DNS is a spectral calculation. This fall off is more pronounced for the wall normal and spanwise components of vorticity and is most likely due to the fact that these components rely on Taylor's hypothesis for the determination of gradients in the streamwise direction.

B. Further tests of local isotropy of the vorticity field

The isotropic spectral relationship between the vorticity components,

$$E_{\omega_y}(k_x) = E_{\omega_z}(k_x) = 1/2[E_{\omega_x}(k_x) - k_x dE_{\omega_x}(k_x)/dk_x], \tag{21}$$

analogous to that for the velocity components, can be easily shown from Eqs. (18)–(20); it is also implied because, like the velocity field, the vorticity field is solenoidal for incompressible flow. This relationship requires that, in a wave number range that is locally isotropic, the ratio of $E^{calc}_{\omega_i}$, from Eq. (21), to $E^{meas}_{\omega_i}$, obtained from direct measurements, must be equal to unity. Here $i=y$ or z. To determine this ratio from our experimental data, the derivative in Eq. (21) was obtained by differentiating a curve fitted through the $E_{\omega_x}(k_x)$ spectrum.

Figure 6 shows this ratio of the calculated cross-stream spectral density values of the vorticity components to their respective measured values. It is apparent that the vorticity field clearly tends toward isotropy near the beginning of the inertial subrange for our data at $k_x\eta \approx 0.01$. The spanwise component approaches the isotropic value of unity at a slightly lower wave number than the wall normal component. Departure from the isotropic value begins at $k_x\eta \approx 0.1$, which is at about the start of the dissipation range. This departure apparently results from the somewhat more rapid roll-off of the E_{ω_y} and E_{ω_z} spectra compared to the E_{ω_x} spectrum in the dissipation range, as seen in Figs. 5(a)–5(c).

From Eq. (21) it is also clear that, in the wave number range where local isotropy holds, the ratios of the measured cross-stream vorticity component spectra, $E^{meas}_{\omega_y}/E^{meas}_{\omega_z}$, must also equal unity. This spectral ratio is shown in Fig. 7. Indeed, the ratio is nearly unity in the inertial subrange. It is also near unity in the dissipation range, but because of the measurement problems noted earlier, the results there are inconclusive.

IV. CONCLUSIONS

A unique experiment to simultaneously measure the velocity vector and the velocity gradient tensor in a very high Reynolds number boundary layer flow was performed in the NASA Ames 80×120 ft^2 wind tunnel. At the measurement location closest to the wall, $y/\delta \approx 0.1$, where the anisotropy of the flow is greatest, both the velocity and vorticity fields exhibit clear indications of local isotropy within the inertial subrange, beginning at $k_x\eta \approx 0.01$, and within the dissipation range up to a nondimensional wave number of $k_x\eta \approx 0.2$ where the probe's inadequate spatial resolution, reliance on a first-order finite difference approximation of the local velocity gradients, and noise and aliasing distort the data. This lower wave number limit for local isotropy is in good quantitative agreement with the streamwise velocity field results of Saddoughi and Veeravalli[9] from measurements obtained simultaneously at the same y/δ location but along the centerline of the tunnel test section.

Our velocity component spectra show good agreement with those of Kim and Antonia[6] from their DNS turbulent channel flow database and with their calculated isotropic spectra in the inertial subrange where there is overlap and into the dissipation range of wave numbers up to $k_x\eta \approx 0.2$. Similar good agreement is found for the vorticity component spectra in the inertial subrange and into the dissipation range

until the measurement limitations mentioned above distort the spectra.

The Reynolds shear stress cospectrum measured with our 12-sensor probe is in very good agreement with that of Saddoughi and Veeravalli.[9] Local isotropy is obtained for a nondimensional mean shear rate of $\epsilon^{1/2}S^{-3/2}k_x \approx 5$.

Further tests of local isotropy were done using the ratio of the calculated [from the one-dimensional $E_{\omega_x}(k_x)$ spectrum] cross-stream vorticity spectra values of $E_{\omega_y}(k_x)$ and $E_{\omega_z}(k_x)$ to their measured values and using the ratio of their measured values themselves. These tests indicate that the vorticity field is locally isotropic in the inertial subrange and in the dissipation range, at least up to the highest wave numbers that the measurements with the probe used in this experiment can be considered resolved and reliable.

ACKNOWLEDGMENTS

The authors would like to extend their appreciation to RACAL Inc. and Howard Harvey of H. Keating Moore and Associates for the loan of the FM tape recorder. The help of S. G. Saddoughi, N. R. Panchapakesan, and J.-L. Balint throughout this difficult experiment is greatly appreciated. Finally we are grateful to E. Balaras and N. Beratlis for help with the figures and their advice about the paper. This research was supported by NSF Grant No. CTS 9217505 and by the Center for Turbulence Research.

[1] A. N. Kolmogorov, "The local structure of turbulence in incompressible viscous fluid for very large Reynolds numbers," C. R. Acad. Sci. URSS **30**, 301 (1941).
[2] C. W. Van Atta, "Local isotropy of the smallest scales of turbulent scalar and velocity fields," Proc. R. Soc. London, Ser. A **434**, 139 (1991).
[3] R. A. Antonia, D. A. Shah, and L. W. B. Browne, "Spectra of velocity derivatives in a turbulent wake," Phys. Fluids **30**, 3455 (1987).
[4] R. A. Antonia, L. W. B. Browne, and D. A. Shah, "Characteristics of vorticity fluctuations in a turbulent wake," J. Fluid Mech. **189**, 349 (1988).
[5] R. A. Antonia, D. A. Shah, and L. W. B. Browne, "Dissipation and vorticity spectra in a turbulent wake," Phys. Fluids **31**, 1805 (1988).
[6] J. Kim and R. A. Antonia, "Isotropy of the small scales of turbulence at low Reynolds number," J. Fluid Mech. **251**, 219 (1993).
[7] R. A. Antonia and J. Kim, "A numerical study of local isotropy of turbulence," Phys. Fluids **6**, 834 (1994).
[8] S. C. Morris and J. F. Foss, "Vorticity spectra in high Reynolds number anisotropic turbulence," Phys. Fluids **17**, 088102 (2005).
[9] S. G. Saddoughi and S. V. Veeravalli, "Local isotropy in high Reynolds number shear flows," J. Fluid Mech. **268**, 333 (1994).
[10] P. Vukoslavčević and J. M. Wallace, "A 12-sensor hot-wire probe to measure the velocity and vorticity vectors in turbulent flow," Meas. Sci. Technol. **7**, 1451 (1996).
[11] F. E. Jorgensen, "Directional sensitivity of wire and fiber film probes," DISA Inf. **11**, 31 (1971).
[12] B. Marasli, P. Nguyen, and J. M. Wallace, "A calibration technique for multiple-sensor hot-wire probes and its application to vorticity measurements in the wake of a circular cylinder," Exp. Fluids **15**, 209 (1993).
[13] G. I. Taylor, "Production and dissipation of vorticity in a turbulent fluid," Proc. R. Soc. London, Ser. A **164**, 15 (1938).
[14] U. Piomelli, J.-L. Balint, and J. M. Wallace, "On the validity of Taylor's hypothesis for wall-bounded turbulent flows," Phys. Fluids A **1**, 609 (1989).